ENVIRONMENTAL RESEARCH
LETTERS

LETTER • OPEN ACCESS

Irrigated cropland expansion exacerbates the urban moist heat stress in northern India

To cite this article: Qiang Guo *et al* 2022 *Environ. Res. Lett.* **17** 054013

ENVIRONMENTAL RESEARCH
LETTERS

OPEN ACCESS

RECEIVED
22 February 2022

REVISED
2 April 2022

ACCEPTED FOR PUBLICATION
6 April 2022

PUBLISHED
25 April 2022

LETTER

Irrigated cropland expansion exacerbates the urban moist heat stress in northern India

Qiang Guo[1,2,*], **Xudong Zhou**[2], **Yusuke Satoh**[3,4] and **Taikan Oki**[1]

[1] Department of Civil Engineering, The University of Tokyo, Tokyo 113-0033, Japan
[2] Institute of Industrial Science, The University of Tokyo, Tokyo 153-8505, Japan
[3] National Institute for Environmental Studies, Tsukuba 305-8506, Japan
[4] International Institute for Applied Systems Analysis, Laxenburg, Austria
[*] Author to whom any correspondence should be addressed.

E-mail: qiang@rainbow.iis.u-tokyo.ac.jp

Keywords: irrigation, moist heat stress, urban, air humidity, wet-bulb temperature

Supplementary material for this article is available online

Abstract

Agricultural irrigation has significantly reshaped the land surface energy and water balance. Previous studies have well investigated its cooling effect on air temperature (T_{air}). However, its effect on increasing air humidity which can intensify the humid heat was often overlooked, particularly over urban areas with high population density, high T_{air}, and consequently greater exposure to moist heat stress. In this study, using state-of-the-art reanalysis data at a high spatial resolution (∼9 km), we evaluated how changes in area equipped for irrigation (AEI) around a city affect urban moist heat stress (UMHS) in more than 1000 cities in China and India. In addition to T_{air}, wet-bulb temperature (T_{WB}) and wet-bulb globe temperature (T_{WBG}), which consider humidity and are closer to the perceived temperature, were assessed. We found that although AEI expansion lowers urban T_{air}, irrigation increases T_{WB} and T_{WBG} due to increased air humidity, thereby exacerbating the UMHS. This 'warming' effect of irrigation is more evident in northern India where AEI has expanded significantly in recent decades, and is prominent in the pre-monsoon and post-monsoon seasons, when precipitation and air humidity are low. However, this effect is not evident in China due to the lower intensity of AEI expansion and differing climatic conditions. Overall, this study highlights the side-effect of irrigation on regional climate, providing crucial information for better understanding urban heat stress and for future city planning.

1. Introduction

Irrigation is one of the most important anthropogenic land management activities, with strong biogeophysical effects on the land surface and regional climate (DeAngelis *et al* 2010, Yang *et al* 2020a). Since the 1950s, to meet the food demands of the rapidly increasing population, the global area equipped for irrigation (AEI) has increased substantially, from 111 Mha in 1950 to 306 Mha in 2005 (Siebert *et al* 2015). In particular, China and India show the largest AEI increases among all countries due to their huge populations (figure S1 available online at stacks.iop.org/ERL/17/054013/mmedia).

Irrigation increases soil moisture and adds additional atmospheric water vapor through evapotranspiration, which reduces the Bowen ratio, lowers surface temperature, increases air humidity, and may also influence regional precipitation. The cooling effects of irrigation on near-surface air temperature (T_{air}) and land surface temperature have been investigated in numerous studies in recent years, using both meteorological observations (Bonfils and Lobell 2007, Yang *et al* 2020a, 2020b) and climate model simulations (Lobell *et al* 2008, Cook *et al* 2010, Kang and Eltahir 2019, Thiery *et al* 2020). Some studies have noted that irrigation can reduce human exposure to heat stress by alleviating extreme T_{air} (Lobell *et al* 2008, Thiery *et al* 2020). However, in recent years, it has been increasingly recognized that the assessment of heat stress should consider not only T_{air}, but also humidity, as high air humidity

prevents humans and livestock from dissipating heat through evaporation of sweat (Pal and Eltahir 2015, Im *et al* 2017, Raymond *et al* 2020). For example, by analyzing 783 cases of heat-related human mortality in 36 countries, Mora *et al* (2017) investigated the climatic conditions associated with human death and found that T_{air} and relative humidity (RH%) are the most important two factors that determine the lethality during heat events. Thus, moist heat stress is closely associated with human health, safety, and productivity risk characterizations (Kjellstrom *et al* 2016, Sherwood 2018).

Wet-bulb temperature (T_{WB}) and wet-bulb globe temperature (T_{WBG}) are two widely used temperature indices that quantify the humid heat in an environment. T_{WB} measures the joint effect of T_{air} and air humidity on the perceived temperature of the human body, while T_{WBG} also considers the influences of wind speed and solar radiation (equations provided in text S1). The values of these two indices are directly correlated with human health and are used to measure the intensity of heat stress. For example, a T_{WB} of 35 °C will cause the cooling mechanism of the human body out of function and result in death within a few hours (Sherwood and Huber 2010, Hanna and Tait 2015). Even a much lower T_{WB} value of 28 °C caused deaths during the 2003 European and 2010 Russian heatwaves (Raymond *et al* 2020). Besides, different T_{WBG} values are also used as thresholds for limiting outdoor military, occupational, and athletic activities (Japan Sports Association 2013).

In recent years, studies have begun to reappraise the impact of irrigation on heat stress through effects on heat and humidity. Kang and Eltahir (2018) and Krakauer *et al* (2020) conducted regional and global climate simulations respectively, with and without irrigation, and found that irrigation tends to increase extreme T_{WB} as well as the intensity and frequency of moist heatwaves. Mishra *et al* (2020) investigated the effects of irrigation on humidity and extreme moist heat stress in India using satellite data and model simulations. They demonstrated that intensive irrigation in India increased air humidity and raised the moist heat stress metrics, indicating impacts on about 37–46 million people in South Asia. However, that study did not explicitly investigate urban areas or the influence of rapid expansion of irrigated cropland.

The effects of irrigation on moist heat stress have not been fully investigated to date, and several key concerns remain unsolved. For example, the few relevant studies have relied on numerical experiments and simply compared simulations with and without irrigation. Even for the state-of-the-art climate models, large biases still exist in these simulations (Guo *et al* 2019, Chen *et al* 2021). Moreover, due to inadequate representation of basic physical processes as well as temporal and spatial discretization, the responses of different models to irrigation may include large uncertainties (Cook *et al* 2014, Fyfe *et al* 2021). Therefore, investigating and verifying the results through examination of *in-situ* and reanalysis data is of great value.

When considering heat and humidity effects, great attention should be paid to urban areas due to the urban heat island effect, high population density, and consequently high risk of moist heat stress (Daniel *et al* 2018, Katzfey *et al* 2020). However, no studies have specifically investigated the effects of irrigation on urban moist heat stress (UMHS). Therefore, using the latest reanalysis and *in-situ* datasets and focusing on urban areas, this study evaluates the effects of irrigated cropland expansion on UMHS for the first time. For more than 1000 cities in China and India that experienced rapid expansions of irrigated cropland and increases in urban population, we investigated the relationship of changes of AEI around cities with UMHS from 1980 to 2005. Moreover, the spatial diversity and the seasonal patterns of irrigation's effect on UMHS are investigated.

2. Data

We used four geophysical, two socio-economic, and two meteorological datasets to calculate AEI expansion around cities and measure its influences on the urban climate. Information about these datasets is provided in table 1. The climate classifications of all cities are shown in figure S2, which is determined by their coordinates (i.e. latitude and longitude) in Kottek *et al* (2006), including 14 climate types in China and 10 climate types in India.

State-of-the-art global reanalysis meteorological data were obtained from ERA5-Land (Munoz-Sabater *et al* 2021), which provides the evolution of land variables with very high temporal (hourly) and spatial (0.1°, ∼9 km) resolution for the period of 1981–2020. T_{air}, dewpoint temperature, downward solar radiation, wind speed, air pressure, and precipitation are used in this study. From the original meteorological variables from ERA5-Land, specific humidity (Q) and relative humidity (RH%) are calculated (text S2). In addition, to validate the reliability of ERA5-Land data, *in-situ* observations of T_{air}, Q, RH%, and T_{WB} from the Hadley Centre Integrated Surface Database (HadISD) (Dunn 2019) are used (text S3 and figures S3–S6).

3. Methods

3.1. Calculation of change in the area equipped for irrigation around each city

To calculate the change in AEI around each city, an impact area is defined for each city. Specifically, a square area around each city (referred to as a city square) is first determined (text S4 and figures S7 and S8), then the AEI proportion (AEI/total area of city square × 100 [%]) and its change from 1980 to 2005 are calculated for each city square. Due to the

Table 1. Information about the datasets used in this study.

Dataset	Spatial resolution	Time range	Time interval	References
Irrigated cropland map	5 arcmin (∼9 km)	1900–2005	5 or 10 year	Siebert *et al* (2015)
European Space Agency Climate Change Initiative land use	300 m	1992–2005	Annual	http://maps.elie.ucl.acbe/CCI/viewer/download.php
City coordinates	Point		Single	https://simplemaps.com/data/world-cities
Köppen–Geiger climate classification	0.5°	1951–2000	Single	Kottek *et al* (2006)
Population	30 arcsec	2010	Single	CIESIN—Columbia University (2018)
Gross domestic product	5 arcmin	2010	Single	Kummu *et al* (2018)
ERA5-Land reanalysis data	0.1° (∼9 km)	1981–2020	Hourly	Munoz-Sabater *et al* (2021)
HadISD *in-situ* meteorological data	Point	1981–2020	Hourly to 6 hour	Dunn (2019)

differing sizes of cities, city square size varies among cities. In general, the size of a city square is approximately ten times the urban area of the city in 2005. In addition, city squares with large water surface areas are excluded from analysis, as water surfaces can have a strong influence on regional air humidity (Condie and Webster 1997). This algorithm obtains the AEI proportion change in each city square for 1036 cities (647 in China and 389 in India).

3.2. Moist heat stress indices

Two indices, wet-bulb temperature (T_{WB}) and wet-bulb globe temperature (T_{WBG}), are used to estimate UMHS. T_{WB} assumes that the skin is completely wet and unclothed, and can be determined as a function of T_{air} and RH% (Stull 2011). T_{WBG} is a more comprehensive index that is the weighted sum of the T_{air}, $T_{WB,}$ and the globe temperature T_G. T_G measures the radiation factor (e.g. solar radiation) in human heat loss and is determined by radiant heat, T_{air}, and wind speed. T_{WBG} applies to realistic conditions of hard exertion when some skin is wet and exposed (Sherwood 2018). The calculation of T_{WBG} in this study is based on Liljegren *et al* (2008). More detailed information on T_{WB} and T_{WBG} and their calculation are provided in text S1.

The UMHS is defined as the intensity and duration of high values of T_{WB} and T_{WBG} over urban areas. We investigated the monthly-average daily maximum T_{WB} and T_{WBG} in each grid that includes a city coordinate at the resolution of ERA5-Land (∼9 × 9 km) to quantify UMHS. The changes of monthly-average daily maximum T_{air}, $T_{WB,}$ and T_{WBG} in the target area are calculated between 1981–1990 and 2001–2010 (the latter period minus the former, hereinafter abbreviated ΔT_{air}, ΔT_{WB}, and ΔT_{WBG}, respectively). In addition to ΔT_{WB} and ΔT_{WBG}, changes in the number of hot days are also evaluated. The number of hot days is defined as the number of days per month on which the daily maximum temperature index values exceed a given threshold: 35 °C, 25 °C, and 31 °C for T_{air}, T_{WB}, and T_{WBG}, respectively. These thresholds are based on previous research (Sherwood and Huber 2010, Japan Sports Association 2013) and represent the warning level that may cause heavy heat stress to the human body.

4. Results

4.1. Change in the area equipped for irrigation around each city

The results show that cities in northwestern India and the North China Plain (NCP) have the highest AEI proportions in 1980, with AEI proportions of some cities being greater than 80% in northwestern India and 60% in the NCP (figure 1(a)). The national average AEI proportions of cities in China and India were 21.5% and 25.3% in 1980, respectively, with India's average value being slightly higher than China's (figure 1(c)).

In terms of changes in AEI proportion between 1980 and 2005 (hereinafter ΔAEI), northern India (mainly the Ganges River basin, hereinafter abbreviated NI) has gone through significant AEI expansion over those 25 years, with ΔAEI in many cities greater than 30% and a regional average ΔAEI of 14.1% (red box 1 in figure 1(b)). In China, apparent AEI expansion also occurred in the NCP, Northeastern China Plain (NECP) (red boxes 2 and 3 in figure 1(b), respectively), some cities in northwestern China (Xinjiang Province), and Inner Mongolia, with increases greater than 20% in a few cities. Regional average ΔAEI in the NCP and NECP are 6.8% and 8.2%, respectively. In general, ΔAEI has been much larger in India than in China, with

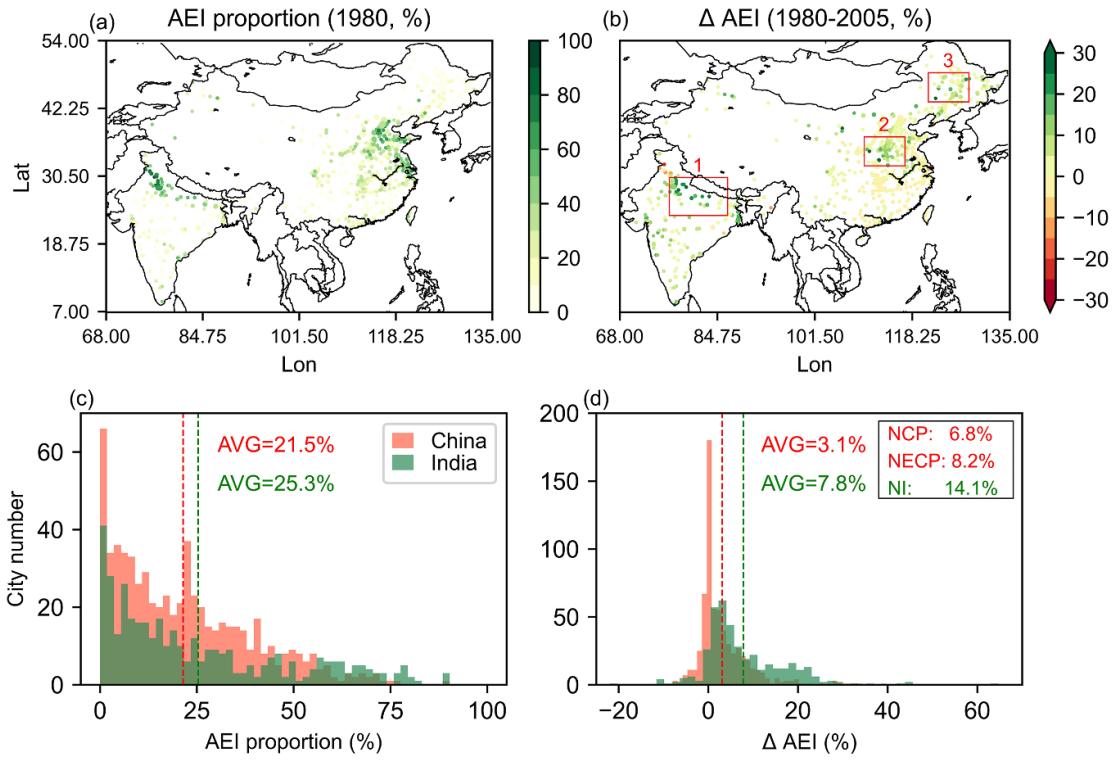

Figure 1. Spatial and frequency distributions of AEI proportion (%) for each city square in China and India in 1980 (a), (c), and its changes (ΔAEI) from 1980 to 2005 (b), (d). The dashed lines and numbers in subplots (c) and (d) indicate the national average values of AEI proportion (c) and ΔAEI (d) in China (red) and India (green), respectively. The red boxes labeled 1–3 in subplot (b) represent NI, NCP, and NECP, respectively, and their regional average ΔAEI values are shown in the box in (d).

national average values of 7.8% and 3.1%, respectively. Moreover, apparent AEI decreases are observed for cities in northwestern India, with the highest AEI proportion occurring in 1980. The maximum AEI proportion decrease of cities in this region is 22.0%.

4.2. Change in urban moist heat stress

We investigated ΔT_{air}, ΔT_{WB}, ΔT_{WBG} (figures 2(a)–(c) and (g)–(i)) and changes in the number of hot days based on these temperature indices (figures 2(d)–(f) and (j)–(l)). The results for the hottest month in China (July) and India (May) are shown. The urban maximum T_{air} in most Chinese cities shows an apparent increase in July (figure 2(a)), and the national average value for all Chinese cities is around 0.5 °C (figure 2(g)). The urban ΔT_{air} values are slightly lower in the NCP and NECP than in other areas (figure 2(g)). In India, however, the ΔT_{air} in May differs among cities located in different regions. The urban maximum T_{air} shows an apparent increase in cities in northwestern India, where an apparent decrease in AEI is observed (figure 1(b)), as well as in the central region near the east coast. By contrast, apparent decreases in urban maximum T_{air} are observed for cities in NI, which have experienced significant AEI expansion, as well as in southern India. In general, the increase of maximum urban T_{air} is not as intense in India as in China, and the national average value for India is around 0 °C. In terms of the number of hot days based on T_{air}, similar changes are observed in regions with significant AEI changes (i.e. NI, NCP, and NECP) as well as in the other regions of each country, except that the increase in hot days in the NECP is slightly smaller than in other regions of China (figure 2(j)).

The results for T_{WB} and T_{WBG} differ from those for T_{air}. Although the apparent cooling of maximum T_{air} is observed in NI, a significant increase in maximum T_{WB} (~0.5 °C) occurs in this region (figure 2(b)). This increase is much larger than the increase in other regions (~0.1 °C) of India (figure 2(h)). This increase of urban maximum T_{WB} in NI is caused mainly by the significant increases in urban maximum Q and RH% (figures S9(a) and (b)). In addition to the increase of daily maximum T_{WB}, the number of hot days based on T_{WB} also shows an apparent increase (~4 d month^{-1}) in NI compared to other regions of India (~1 d month^{-1}). However, for cities in China, no difference in ΔT_{WB} is evident between regions with apparent AEI increases (NCP and NECP) and other regions. Furthermore, due to the decrease of Q in the NECP (figure S9(a)), its maximum T_{WB} and number of hot days show slight decreases.

For T_{WBG}, which further considers downward solar radiation and wind speed, similar results to T_{WB} were observed in both China and India. The increases in maximum daily T_{WBG} and the corresponding

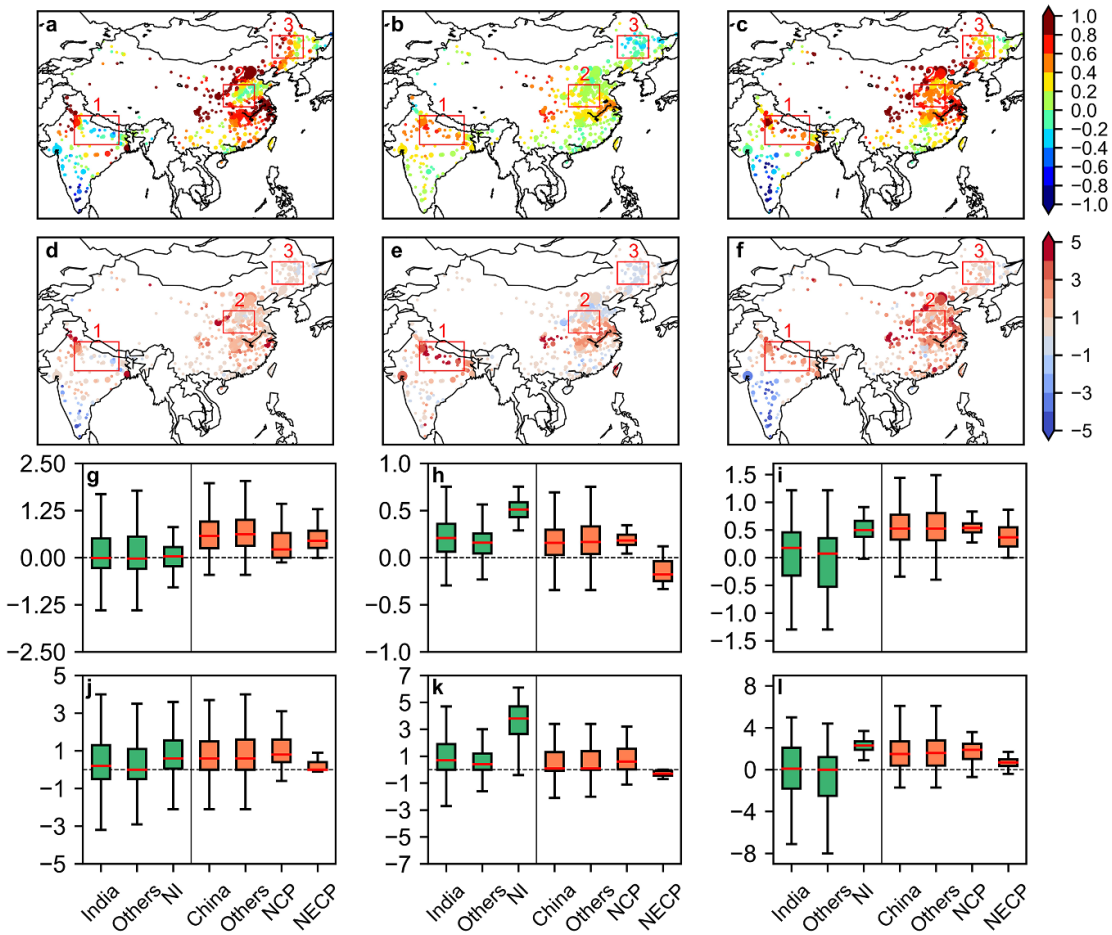

Figure 2. The changes in average daily maximum T_{air}, T_{WB}, and T_{WBG} (ΔT_{air}, ΔT_{WB}, and ΔT_{WBG}, °C) (a)–(c) and their corresponding hot days (d month^{-1}) (d)–(f) in the urban area of each city between 1981–1990 and 2000–2010; boxplots of ΔT_{air}, ΔT_{WB}, and ΔT_{WBG} (°C) (g)–(i) and their corresponding hot days (d month^{-1}) changes (j)–(l) in different regions. On the *x*-axis label in (j)–(l), 'Others' represents the other cities excluding NI (for India), NCP, and NECP (for China). The results of the hottest month are shown for China (July) and India (May).

number of hot days in NI are much greater than in other regions in India (figures 2(c), (f), (i) and (l)). The time series of T_{air}, Q, T_{WB}, and T_{WBG} for cities in India also indicate that cities in NI experienced apparent T_{air} cooling along with significant increases of Q, T_{WB}, and T_{WBG} compared with other regions (figure S10).

4.3. Correlation between expansion of the area equipped for irrigation and changes in urban moist heat stress

To investigate the relationship between AEI expansion and UMHS changes in recent decades, we analyzed the correlations of ΔT_{air}, ΔT_{WB}, and ΔT_{WBG} with ΔAEI in NI, NCP, and NECP. The corresponding Spearman correlation coefficients are denoted as the ΔT_{air}-ΔAEI, ΔT_{WB}-ΔAEI, and ΔT_{WBG}-ΔAEI correlation coefficients, respectively. Figure 3 shows a scatterplot of temperature metric changes versus ΔAEI for cities located in NI, NCP, and NECP. Due to the differing climatic conditions of these cities, the results are presented separately for each climate classification, including Csa (warm temperate, summer dry, hot summer), Cwa (warm temperate, winter dry, hot summer), and Dwa (snow, winter dry, hot summer). The AEI changes of cities under each climate classification in China and India are shown in figure S11.

For cities in NI, the ΔT_{air} values show significant negative correlations (p-value $\leqslant 0.01$) with ΔAEI in the surrounding area (figures 3(a) and (b)). The ΔT_{air}-ΔAEI correlation coefficients for Csa and Cwa in NI are −0.56 and −0.31, respectively. By contrast, ΔT_{WB} and ΔT_{WBG} in urban areas show positive correlations (p-value $\leqslant 0.01$) with ΔAEI, with ΔT_{WB}-ΔAEI and ΔT_{WBG}-ΔAEI correlation coefficients for both climate classifications greater than 0.5. These results indicate that the increase of AEI in the NI region tends to reduce the daily maximum urban T_{air} in the hottest month, but, intensified irrigation activities also affect other climate variables (e.g. increased air humidity), which increases the risks of moist heat stress in urban areas.

However, this phenomenon is not evident in the NCP and NECP regions of China, and the corresponding correlation coefficients between

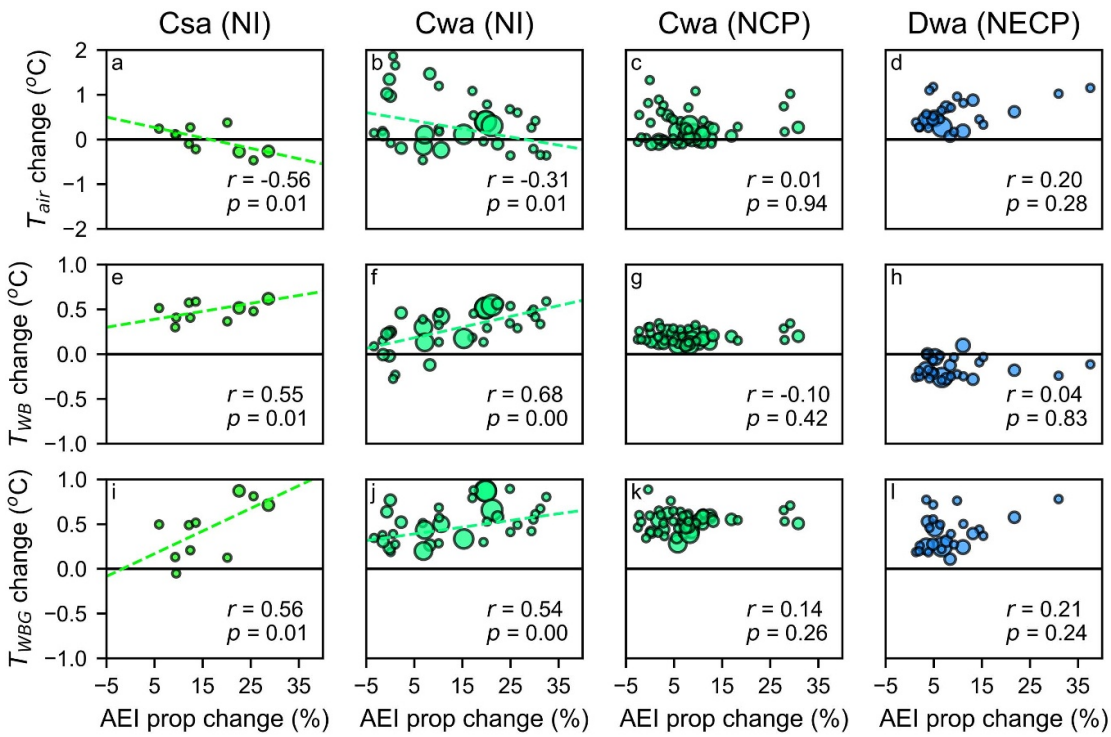

Figure 3. Scatterplots of ΔT_{air} (a)–(d), ΔT_{WB} (e)–(h), ΔT_{WBG} (i)–(l) between 1981–1990 and 2000–2010 (*y*-axis) versus ΔAEI from 1980 to 2005 (*x*-axis) for cities under four Köppen–Geiger climate classifications located in NI, NCP, and NECP. Each dot represents the result for one city; the dot size indicates the city square size. The dot color is consistent with the climate classification in figure S2. The results for the hottest month in China (July) and India (May) are shown. *r* and *p* represent the Spearman correlation coefficient and the corresponding *p*-value, respectively.

temperature metric changes and ΔAEI are low (figures 3(c), (d), (g), (h), (k) and (l)). This difference between India and China may result from the following four factors. First, the expansion of AEI is more significant for cities in NI. The average value of ΔAEI in NI is approximately double those in NCP and NECP. This difference makes AEI expansion a more critical factor in shaping the regional climate in NI than in the other areas. Second, the impact of artificial moisture supply from irrigation should be greater under drier conditions. The air is much drier in NI in May (with RH% around 20%–40%) than in the NCP and NECP in July (with RH% around 60%–80%) (figure S12). Third, NI may have larger irrigation water consumption compared with NCP and NECP. For example, Siebert and Döll (2010) showed that the annual irrigation consumption in NI (mainly 400–1922 mm yr^{-1}) is apparently higher than NCP and NECP (mainly 250–600 mm yr^{-1} and 150–400 mm yr^{-1}, respectively). In addition, the difference in regional irrigation method/efficiency may also influence. For example, Fu *et al* (2022) found that by implementing water-saving techniques, irrigation water use has been substantially reduced in Northwest China in recent decades, which mitigates the influence of irrigation on regional evapotranspiration, temperature, and humidity. Similarly, such water-saving techniques are also substantially applied in NCP and apparent improvement in irrigation efficiency is found in NCP in recent decades (Zhou *et al* 2020). Forth, for cities of the NCP and NECP regions, other factors such as urban area expansion and global warming may have strong impacts on the regional climate that mask the influence of AEI expansion.

To further investigate the seasonal variation of the effect of AEI expansion on daily maximum urban T_{air} and UMHS, the ΔT_{air}-ΔAEI, ΔT_{WB}-ΔAEI, and ΔT_{WBG}-ΔAEI correlation coefficients for 12 months are plotted in figure 4. Only correlation coefficients that meet the significant criterion (*p*-value < 0.05) are shown in color. The results indicate that the cooling effect of AEI expansion on urban T_{air} generally occurs throughout the year in Cwa climate zones in NI, while it is apparent only during winter (November–February) and the pre-and early-monsoon (May–June) seasons in Csa zones in NI. These results are in accordance with the findings of Mishra *et al* (2020), who reported that irrigation-induced cooling is more dominant during the pre-monsoon and post-monsoon seasons in NI based on satellite data. For T_{WB}, the enhancement driven by AEI expansion is most apparent during the pre- and early-monsoon seasons (February–June) for both Cwa and Csa climate zones in NI and during the post-monsoon season (October–November) for Cwa. In monsoon months with abundant precipitation and air humidity, the effect of AEI expansion on

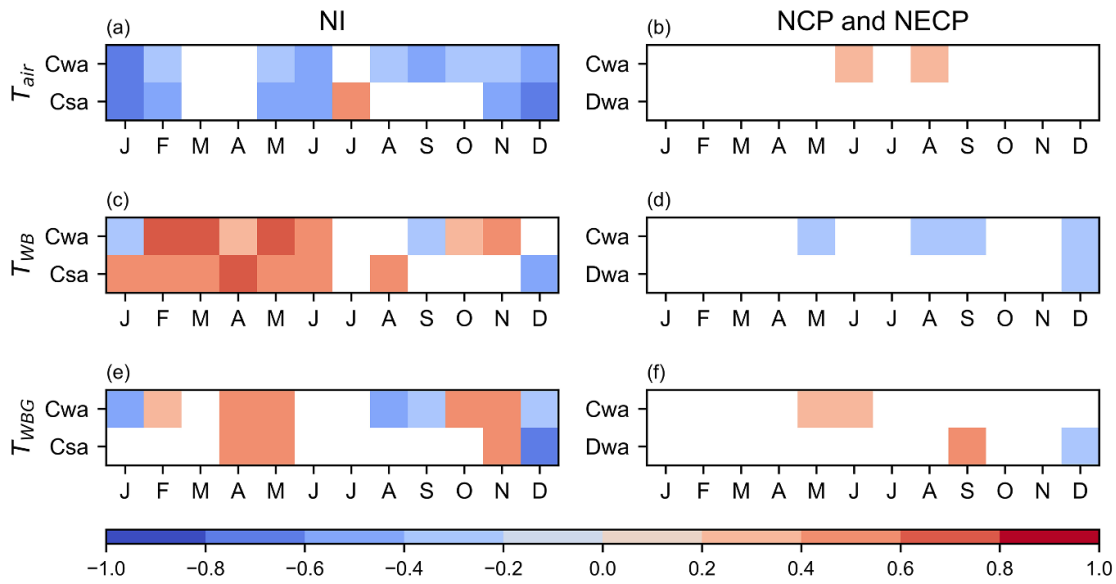

Figure 4. Heatmap of Spearman correlation coefficients between the changes in three temperature indices (daily maximum T_{air} (a), (b), T_{WB} (c), (d), and T_{WBG} (e), (f)) between 1981–1990 and 2000–2010 and ΔAEI from 1980 to 2005 in cities under four Köppen–Geiger climate classifications in NI (Cwa and Csa in (a), (c), (e)), NCP (Cwa in (b), (d), (f)), and NECP (Dwa in (b), (d), (f)) for 12 months.

UMHS is insignificant. Similar to T_{WB}, the influence of AEI expansion on T_{WBG} in NI is stronger in the pre-monsoon (April–May) and post-monsoon (October–November) seasons. In the NCP (Cwa) and NECP (Dwa) regions of China, the effect of AEI expansion on maximum urban T_{air} and UMHS is unclear, and no seasonal variation pattern can be identified.

To directly evaluate the correlations between ΔAEI and influencing factors of moist heat metrics, heatmaps of correlation coefficients of ΔAEI with the change in daily maximum Q, solar radiation, wind speed, and daytime mean RH% in urban areas were constructed (figure S13). Changes in Q and RH% in NI show strong positive correlations with AEI expansion during the pre-and early-monsoon season (January–June) and the post-monsoon season (October–November). In addition, wind speed change shows negative correlations with AEI expansion in NI (March–June, September–December), which may be driven by the increased roughness of the land surface caused by cropland expansion around the city. The change in solar radiation has no apparent correlation with AEI expansion.

4.4. Relative contribution of the area equipped for irrigation expansion to urban moist heat stress

In addition to AEI change, changes in urbanized areas and regional precipitation may also affect urban T_{air} and humidity. Changes in the urban area proportion of each city square and regional precipitation in recent decades are shown in figures S14 and S15, respectively. To evaluate the contributions of AEI expansion to UMHS compared with those two factors, we applied multivariate linear regression to fit urban ΔT_{air}, ΔQ, and ΔT_{WB} as functions of ΔAEI, urban area proportion change (ΔUA), and precipitation change (ΔP) (text S5). Using the fitted regression model, the contribution of each factor to urban ΔT_{air}, ΔQ, and ΔT_{WB} can be measured based on a change (increase) of one standard deviation for each factor. The regression model was fitted for 70 cities under the Cwa climate in NI in May, which is both the hottest month and when UMHS changes have strong correlations with ΔAEI (as shown in figures 4 and S13).

Figure 5 shows the performance of the regression models (a)–(c) and the contribution of each factor to the output (d)–(f). The results indicate that the regression model can accurately simulate metrics changes from ERA5-Land data and that the variability of metric changes is explained well by three input factors, all of which have R^2 values near or greater than 0.5. Moreover, the regression models have small root mean square error (RMSE) values. In terms of the contribution of each factor to the metrics changes, an increase in urban area proportion tends to increase urban maximum T_{air} in NI, while increases in AEI and precipitation tend to decrease urban maximum T_{air}, with increased precipitation showing a larger cooling effect on T_{air} than ΔAEI. For ΔQ and ΔT_{WB}, increases in both AEI and precipitation tend to increase urban maximum Q and T_{WB}, with AEI expansion making the larger contribution to the increases of Q and T_{WB}. An increase in urban areas has a slight negative effect on Q, and its impact on T_{WB} is negligible compared to the effects of AEI expansion and increased precipitation.

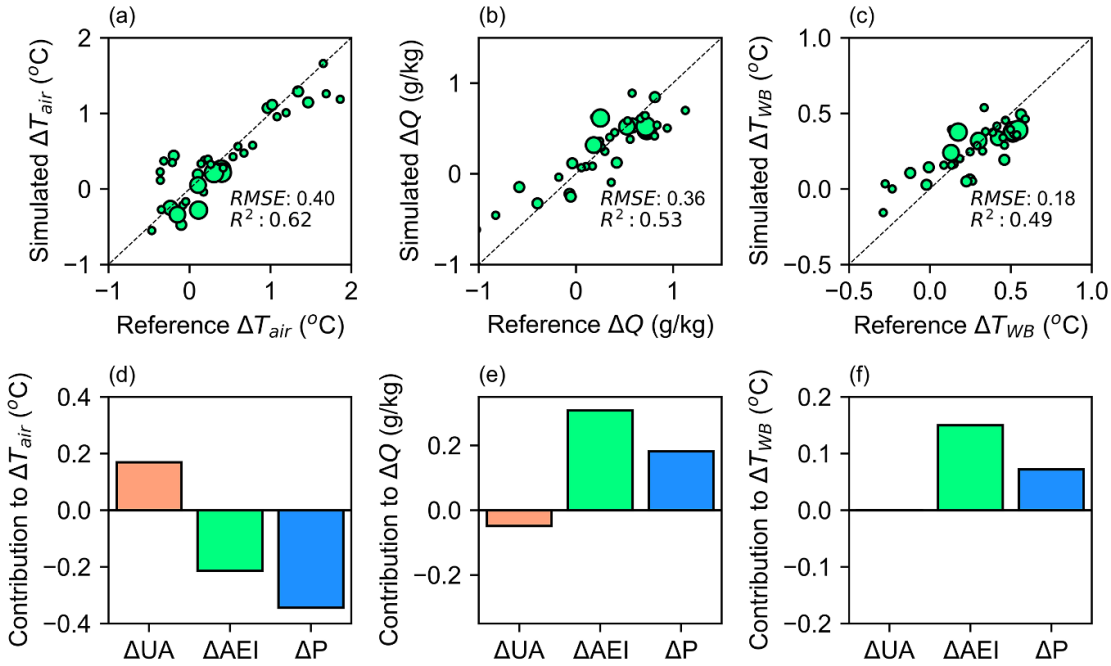

Figure 5. (a)–(c) Scatterplots of urban ΔT_{air}, ΔQ, and ΔT_{WB} simulated with a multivariate regression model versus corresponding reference data from ERA5-Land for each city in the Cwa climate zone in NI. RMSE and R^2 indicate root mean square error and coefficient of determination, respectively. (d)–(f) Relative contributions of changes of one standard deviation in urban area proportion (ΔUA, 3.9%), AEI proportion (ΔAEI, 13.1%) and precipitation (Δ*P*, 21.7%, 18 mm) to ΔT_{air}, ΔQ, and ΔT_{WB}.

4.5. Verifying results with HadISD *in-situ* data

For validation, we investigated the changes in daily maximum T_{air}, Q, T_{WB}, and daily average RH% of the hottest month between the periods of 1981–1990 and 2001–2010 at 372 stations in China and 72 stations in India using the HadISD dataset (figure S16). Although climate stations have a much lower density than cities, especially in India, similar regional patterns can be observed. In addition, despite the cooling of T_{air} in NI is less evident in the station data than in reanalysis data due to the influences of local conditions around the station and the low station density, much greater increases of air humidity and T_{WB} are observed in NI than in other regions of India. These results indicate that NI has experienced a strong intensification of moist heat stress in recent decades. As NI has the highest population density in India and very high gross domestic product (figure S17), the enhancement of UMHS due to AEI expansion may lead to high exposure and risk for outdoor workers, impacting economic activities.

5. Discussion

The near-surface meteorological variables of ERA5-Land are used to conduct the main analysis, which uses similar data inputs with ERA5 that combines multi-source observations and model forecasts. Admittedly, assumptions and inadequacies of the model may induce biases to the outputs (Singh *et al* 2021), which may also partly result in its deviation with respect to ground-based observations (figure S16). However, vast amounts of radiosonde, satellite-based, and *in-situ* observations are assimilated into the estimation to obtain the most plausible state of the atmosphere. For example, in terms of near-surface field, from 1979 to 2019, there are about one billion observations for each of surface air temperature and relative humidity were processed by the land data assimilation module of ERA5-Land (Hersbach *et al* 2020). The assimilated data with these comprehensive observations can well reflect the time-evolving and the spatial diversity of the near-surface climate state, which provides reliable support to measure the influence of AEI change on regional climate.

The Köppen–Geiger climate classification of Kottek *et al* (2006) is used to classify the cities when conducting correlation analysis, which represents the climate state of 1951–2000. Admittedly, the climate classification is changing under global warming, and some updated versions of Köppen–Geiger climate classification with higher-resolution were proposed based on different input datasets (Beck *et al* 2018). However, the focus of our research is to detect the influence of irrigation in specific regions with intensive irrigated cropland expansion (e.g. NI), and the climate classification is only used to mitigate the potential influence of climate difference in correlation analysis. Therefore, although there are various versions of climate classifications, we believe it will not change our results and conclusions in how irrigated

cropland expansion influences the region and urban climates.

Notably, changes in UMHS can be influenced by global warming and internal climate variability in addition to the regional influence of AEI expansion (Im *et al* 2017, Mishra *et al* 2020). For example, El Niño–Southern Oscillation affects monsoon systems, altering temperature and humidity in India and China (Revadekar *et al* 2009, Zhang *et al* 2018, Kiran Kumar and Singh 2021). Nonetheless, the main objective of this study is investigating the influence of AEI expansion on UMHS. In-depth quantification of the contributions of various factors influencing temperature and humidity in these regions is a critical research direction for future studies.

In addition to moisture from anthropogenic irrigation activities, urbanization can lead to additional anthropogenic moisture emissions through multiple pathways (e.g. thermal power plants), with effects on humidity. In this study, the specific humidity Q is negatively correlated with ΔUA in NI, demonstrating an urban dry island effect (Hao *et al* 2018). However, the influence of urbanization on humidity remains under debate and opposing results have been obtained in different cities (known as urban wet and dry island effects) (Wang and Gong 2010, Sailor 2011, Hao *et al* 2018). Future comprehensive analyses of UMHS should consider these effects.

6. Conclusions

This study presents novel findings regarding the influence of irrigated cropland expansion around cities on UMHS in more than 1000 cities in India and China. Using state-of-the-art reanalysis and *in-situ* climate data, we conducted the first analysis focused specifically on urban areas and found that during 1980–2005, cities in NI, NCP, and NECP have experienced significant increases in the AEI in their suburb areas of 14.1%, 6.8%, and 8.2%, respectively. In NI, AEI expansion tends to result in urban T_{air} cooling. Conversely, as irrigation activity increases air humidity, AEI expansion shows positive correlations with the increases of T_{WB} and T_{WBG}, indicating enhancement of the UMHS. This effect is most apparent in the pre-monsoon and post-monsoon seasons, when precipitation is low. However, no such effects of AEI expansion are observed for cities in NCP and NECP in China due to the differences in AEI expansion intensity and climatic conditions. The results of multivariate linear regression analysis support AEI expansion having stronger impacts on exacerbating the UMHS than precipitation changes and urban area expansion in NI over recent decades.

Data availability statement

The data that support the findings of this study are available upon reasonable request from the authors.

Acknowledgments

This work was partially supported by the Japan Society for the Promotion of Science (KAKENHI: 16H06291 and 21H05002), and the Environment Research and Technology Development Fund of the Environmental Restoration and Conservation Agency of Japan, Grant Number JPMEERF20202005. The author would like to thank Dr Seibert at the University of Bonn for making their irrigated cropland map dataset available. The author would like to thank the developer and contributor of ERA5-Land, HadISD, CCI land cover, World Cities datasets.

ORCID iDs

Qiang Guo https://orcid.org/0000-0001-6539-5988
Yusuke Satoh https://orcid.org/0000-0001-6419-7330

References

Beck H E, Zimmermann N E, McVicar T R, Vergopolan N, Berg A and Wood E F 2018 Present and future Köppen-Geiger climate classification maps at 1-km resolution *Sci. Data* **5** 180214

Bonfils C and Lobell D 2007 Empirical evidence for a recent slowdown in irrigation-induced cooling *Proc. Natl Acad. Sci. USA* **104** 13582–7

Chen J, Arsenault R, Brissette F P and Zhang S 2021 Climate change impact studies: should we bias correct climate model outputs or post-process impact model outputs? *Water Resour. Res.* **57** e2020WR028638

CIESIN—Columbia University 2018 *Gridded Population of the World, Version 4 (GPWv4): Population Density, Revision 11* (https://doi.org/10.7927/H49C6VHW)

Condie S A and Webster I T 1997 The influence of wind stress, temperature, and humidity gradients on evaporation from reservoirs *Water Resour. Res.* **33** 2813–22

Cook B I, Puma M J and Krakauer N Y 2010 Irrigation induced surface cooling in the context of modern and increased greenhouse gas forcing *Clim. Dyn.* **37** 1587–600

Cook B I, Shukla S P, Puma M J and Nazarenko L S 2014 Irrigation as an historical climate forcing *Clim. Dyn.* **44** 1715–30

Daniel M, Lemonsu A, Déqué M, Somot S, Alias A and Masson V 2018 Benefits of explicit urban parameterization in regional climate modeling to study climate and city interactions *Clim. Dyn.* **52** 2745–64

DeAngelis A, Dominguez F, Fan Y, Robock A, Kustu M D and Robinson D 2010 Evidence of enhanced precipitation due to irrigation over the Great Plains of the United States *J. Geophys. Res.* **115** D15115

Dunn R J H 2019 HadISD version 3: monthly updates

Fu J, Kang S, Zhang L, Li X, Gentine P and Niu J 2022 Amplified warming induced by large-scale application of water-saving techniques *Environ. Res. Lett.* **17** 034018

Fyfe J C, Kharin V V, Santer B D, Cole J N S and Gillett N P 2021 Significant impact of forcing uncertainty in a large ensemble of climate model simulations *Proc. Natl Acad. Sci. USA* **118** e2016549118

Guo Q, Chen J, Zhang X, Shen M, Chen H and Guo S 2019 A new two-stage multivariate quantile mapping method for bias correcting climate model outputs *Clim. Dyn.* **53** 3603–23

Hanna E G and Tait P W 2015 Limitations to thermoregulation and acclimatization challenge human adaptation to global warming *Int. J. Environ. Res. Public Health* **12** 8034–74

Hao L, Huang X, Qin M, Liu Y, Li W and Sun G 2018 Ecohydrological processes explain urban dry island effects in a Wet Region, Southern China *Water Resour. Res.* **54** 6757–71
Hersbach H, Bell B, Berrisford P, Hirahara S, Horányi A, Muñoz-Sabater J and Thépaut J N 2020 The ERA5 global reanalysis *Q. J. R. Meteorol. Soc.* **146** 1999–2049
Im E S, Pal J S and Eltahir E A B 2017 Deadly heat waves projected in the densely populated agricultural regions of South Asia *Sci. Adv.* **3** e1603322
Japan Sports Association 2013 *A Guidebook for the Prevention of Heat Disorder during Sports Activities* 4 edn (Tokyo: Japan Sports Association)
Kang S and Eltahir E A B 2018 North China Plain threatened by deadly heatwaves due to climate change and irrigation *Nat. Commun.* **9** 2894
Kang S and Eltahir E A B 2019 Impact of irrigation on regional climate over Eastern China *Geophys. Res. Lett.* **46** 5499–505
Katzfey J, Schlünzen H, Hoffmann P and Thatcher M 2020 How an urban parameterization affects a high-resolution global climate simulation *Q. J. R. Meteorol. Soc.* **146** 3808–29
Kiran Kumar P and Singh A 2021 Increase in summer monsoon rainfall over the northeast India during El Niño years since 1600 *Clim. Dyn.* **57** 851–63
Kjellstrom T, Briggs D, Freyberg C, Lemke B, Otto M and Hyatt O 2016 Heat, human performance, and occupational health: a key issue for the assessment of global climate change impacts *Annu. Rev. Public Health* **37** 97–112
Kottek M, Grieser J, Beck C, Rudolf B and Rubel F 2006 World Map of the Köppen-Geiger climate classification updated *Meteorol. Z.* **15** 259–63
Krakauer N Y, Cook B I and Puma M J 2020 Effect of irrigation on humid heat extremes *Environ. Res. Lett.* **15** 094010
Kummu M, Taka M and Guillaume J H A 2018 Gridded global datasets for gross domestic product and human development index over 1990–2015 *Sci. Data* **5** 180004
Liljegren J C, Carhart R A, Lawday P, Tschopp S and Sharp R 2008 Modeling the wet bulb globe temperature using standard meteorological measurements *J. Occup. Environ. Hyg.* **5** 645–55
Lobell D B, Bonfils C J, Kueppers L M and Snyder M A 2008 Irrigation cooling effect on temperature and heat index extremes *Geophys. Res. Lett.* **35** L09705
Mishra V, Ambika A K, Asoka A, Aadhar S, Buzan J, Kumar R and Huber M 2020 Moist heat stress extremes in India enhanced by irrigation *Nat. Geosci.* **13** 722–8
Mora C, Dousset B, Caldwell I R, Powell F E, Geronimo R C, Bielecki C R and Trauernicht C 2017 Global risk of deadly heat *Nat. Clim. Change* **7** 501–6
Munoz-Sabater J, Dutra E, Agusti-Panareda A, Albergel C, Arduini G, Balsamo G and Thepaut J N 2021 ERA5-Land: a state-of-the-art global reanalysis dataset for land applications *Earth Syst. Sci. Data* **13** 4349–83
Pal J S and Eltahir E A B 2015 Future temperature in southwest Asia projected to exceed a threshold for human adaptability *Nat. Clim. Change* **6** 197–200
Raymond C, Matthews T and Horton R M 2020 The emergence of heat and humidity too severe for human tolerance *Sci. Adv.* **6** eaaw1838
Revadekar J V, Kothawale D R and Rupa Kumar K 2009 Role of El Niño/La Niña in temperature extremes over India *Int. J. Climatol.* **29** 2121–9
Sailor D J 2011 A review of methods for estimating anthropogenic heat and moisture emissions in the urban environment *Int. J. Climatol.* **31** 189–99
Sherwood S C 2018 How important is humidity in heat stress? *J. Geophys. Res.* **123** 11808–10
Sherwood S C and Huber M 2010 An adaptability limit to climate change due to heat stress *Proc. Natl Acad. Sci. USA* **107** 9552–5
Siebert S and Döll P 2010 Quantifying blue and green virtual water contents in global crop production as well as potential production losses without irrigation *J. Hydrol.* **384** 198–217
Siebert S, Kummu M, Porkka M, Döll P, Ramankutty N and Scanlon B R 2015 A global data set of the extent of irrigated land from 1900 to 2005 *Hydrol. Earth Syst. Sci.* **19** 1521–45
Singh T, Saha U, Prasad V S and Gupta M D 2021 Assessment of newly-developed high resolution reanalyses (IMDAA, NGFS and ERA5) against rainfall observations for Indian region *Atmos. Res.* **259** 105679
Stull R 2011 Wet-bulb temperature from relative humidity and air temperature *J. Appl. Meteorol. Climatol.* **50** 2267–9
Thiery W, Visser A J, Fischer E M, Hauser M, Hirsch A L, Lawrence D M and Seneviratne S I 2020 Warming of hot extremes alleviated by expanding irrigation *Nat. Commun.* **11** 290
Wang X and Gong Y 2010 The impact of an urban dry island on the summer heat wave and sultry weather in Beijing City *Chin. Sci. Bull.* **55** 1657–61
Yang Q, Huang X and Tang Q 2020a Global assessment of the impact of irrigation on land surface temperature *Sci. Bull.* **65** 1440–3
Yang Q, Huang X and Tang Q 2020b Irrigation cooling effect on land surface temperature across China based on satellite observations *Sci. Total Environ.* **705** 135984
Zhang L, Wu P, Zhou T and Xiao C 2018 ENSO transition from La Niña to El Niño drives prolonged spring–summer drought over North China *J. Clim.* **31** 3509–23
Zhou F, Bo Y, Ciais P, Dumas P, Tang Q, Wang X and Wada Y 2020 Deceleration of China's human water use and its key drivers *Proc. Natl Acad. Sci. USA* **117** 7702–11